Resolution limits for mapping roots with GPR: a numerical modeling study

ROCHA[1], Amanda Almeida; MACIEL[2], Susanne Tainá Ramalho; AGUIAR[3], Guilherme Zakarewicz; BORGES[2], Welitom Rodrigues.
[1]: Mestranda no Programa de Pós Graduação em Geociências Aplicadas Universidade de Brasília; [2] : Professor Adjunto Universidade de Brasília; [3]: Graduando em Geofísica Universidade de Brasília.

Abstract

Trees are important functions in the ecosystem for being able to storage atmospheric CO_2 to increase its biomass. Roots are significant and indispensable for the ecosystem carbon budget, accounting for 20-40% of the total forest carbon storage (Cui *et al.* 2011). Traditional techniques used for forest engineers to quantify root biomass are destructive, laborious and time demanding.

Over the last decades since Hruska (1999), GPR has been studied to map efficiently coarse roots biomass, due to its non-destructive nature and fast data acquisition capability.

Numerical modeling provides a faster alternative to study the limiting factors of GPR-based root investigation when compared to controlled experiments. Therefore the application of numerical modeling to understand the influences of limiting factors on both the detection and quantification of roots by GPR is promising.

This paper shows satisfactorily the accuracy of numerical modeling using the software Reflexw(R) and its feasibility in exploring the impacts of limiting factors on root diameter and root water content variation for the transverse electric field and the transverse magnetic field.

Introduction

GPR has been studied over the last decades to map efficiently coarse roots biomass, due to its non-destructive nature and fast data acquisition capability. GPR is a geophysical technique widely used for detecting materials within shallow subsurface (Conyers, 2004). It uses contrasts in reflected electromagnetic waves to map the subsoil.

Although the accuracy of root biomass estimation is still unsatisfactory because current models use information from reflective energy of each site-specific to calculate root biomass. It is necessary to understand better the various limiting factors to enhance the application of GPR.

The radar signal is significantly affected by many biotic factors (e.g. root diameter, root water content, roots spacing and root orientation) and abiotic variables (e.g. soil water content, soil texture, soil surface condition and antenna center frequency) (Barton and Montagu 2004; Dannoura *et al.* 2008; Hirano *et al.* 2009; Guo *et al.* 2013).

The depth of groundwave penetration decreases with increasing frequency and increased soil moisture, which affects ε_{soil} and considerably change the velocity model, according to Du & Rummel (1994).

The penetration depth is higher in dry soils and dry rocks, and considerably lower in moist and loamy soils, since both have high electrical conductivity (Wensink *et al.*, 1993).

Numerical modeling provides a faster alternative to study the limiting factors of GPR-based root investigation when compared to controlled experiments. Since all the variables in the simulation model can be precisely controlled it is possible to differentiate and to detect the various limiting factors (Guo *et al.* 2013).

Therefore the application of numerical modeling to understand the influences of limiting factors on both the detection and quantification of roots by GPR is promising.

The objective of this work is to analyse how the diameter of the target root and its water content variation impacts the resolution limit for the transverse electric field and the magnetic field in synthetic data.

Method

A GPR processing routine was established to process 16 synthetic radargrams. The radargrams were generated by Reflexw using different diameters of sample targets and different dielectric constants for sample targets.

The nature of the GPR forward problem can be classified as an initial value-open boundary problem. Then, in order to obtain a solution, one has to define an initial condition (i.e., frequency of the GPR transmitting antenna) and allow for the resulting fields to propagate through space, reaching – in theory – a zero value at infinity.

The specification of the source is required. Three main constants are used for both materials (in this case root and sand) to build a numerical modeling in Reflexw: ε (dielectric permittivity); μ (magnetic permeability) and σ (electrical conductivity). The main parameters used to model were established by al-Hagrey (2007), Annan (1992) and Torgonivkov (1992) in **Table 1**.

The finite-difference time-domain method cannot assign the values of dx, dy and dz independently, it is a conditionally stable numerical process. The stability condition is known as the CFL condition (Taflove, 1995) and is given by:

$$dt \leq \frac{1}{c\sqrt{\frac{1}{(dx)^2}+\frac{1}{(dy)^2}+\frac{1}{(dz)^2}}} \quad (1)$$

where *c* is the speed of light. Hence, *dt* is bounded by the values of *dx*, *dy* and *dz*. The stability condition for the 2D case is easily obtained by letting $dz \rightarrow \infty$.

Material		ε	σ (S/m)	v(m/ns)	(dB/m)
Soil [sandy-loamy]	dry saturated	3-7 15-30	0.0001-0.1 0.01-1	0.11-0.18 0.05-0.09	0.01-0.1 0.03-0.3
Wood cellulose	dry saturated	4.5 22	0.00024 0.004	0.141 0.064	0.187 1.35
Clays	-	5-40	0.002-1	0.06	1-300
Water	fresh	80	0.0005	0.033	0.1
Air	dry	1	0	0.3	0

Table 1 - Dielectric characteristics of common materials (al Hagrey 2007, Annan 1992, Torgovnikov 1992).

It is important to note that the spacial increment 'dx' is related to the minimum wavelength present in the medium (Taflove, 1995), this increment must be 10 times smaller than the smallest wavelength existent in the system. Errors in the spacial and temporal parameters choice could bring on numerical dispersion (Sandmeier, 2015).

For the boundary conditions absorbent it was established the parameters '*linear absorbing range*', which is expressed by the equation:

$$\sigma_{\text{end}} = \text{fac}\ \omega\ \varepsilon_{\text{act}}\ \varepsilon_0 \quad (2)$$

where, σ_{end} is the final conductivity in relation to ε_{act}; ω is the angular frequency ; ε_{act} is the actual value of ε of the model's last point before the boundary; ε_0 is the vacuum dielectric permittivity; fac = Size/50 , where Size is the number of points in the grid.

The antenna polarization used in the modeling were configured simulating the source transmitter with the dominant component Ey (Ey-Ey), transverse electric (TE), then the source used was the Ex component with the registration in (Ex-Ex), which represents the transverse magnetic (TM).

Simulating the reflections of the electromagnetic wave (Ey-Ey and Ex-Ex) by the surface of the reflector was used as the electromagnetic source the mode 'exploding reflector', which is characterized by the emission of the wavefront scattered directly by the target towards surface. This source is equivalent to the step of data migration (Yilmaz, 1987). This kind of source allows you to simulate a 2D zero offset section which means that we started the time at t = 0, all points originating from a reflector are the starting points of an elementary wave of Huygens with an amplitude proportional to the reflection coefficient for the case of an incidence (Sandmeier, 2015).

The same processing steps was applied for all data acquired. The data was processed through the software Reflexw v. 7.5 (Sandmeier, 2015).

The processing flow applied was the addition of noise of 10%. The butterworth bandpass filter used had a lower cutoff of 2100MHz and a upper cutoff of 3200MHz.

Resolution Limits

The resolution capability of the GPR depends basically on the frequency of the antenna used, the depth of the target object, the dielectric constant of the medium and the dielectric constant of the target.

The shorter wavelengths of high centre frequency antennas produce narrower cone of transmission, which can focus on smaller areas and thereby resolve smaller features than the more spread out transmission cones produced by antennas with low centre frequencies and longer wavelengths (Conyers 2004).

Here it is important to explain that the GPR produces EM waves in a broadband, such that frequencies from one half to two times that of the centre frequency are present (Annan 2009).

In general, the maximum resolution of horizontal features is roughly equivalent to the coverage area (**Figure 2**) given by Conyers & Goodman (1997):

$$A = \frac{\lambda}{4} + \frac{D}{\sqrt{\varepsilon+1}}, \quad (3)$$

where *A* is the long dimension of the elliptical footprint; λ is the wavelength of the central frequency of the radar; *D* is the depth and ε is the medium dielectric permittivity.

The maximum resolvable horizontal target is equivalent to A, the long dimension of the footprint (Conyers 2004).

The maximum resolution of vertical features is roughly equivalent to or larger than half the wavelength (Neubauer *et al.* 2002). Vertically stacked horizontal interfaces must be separated by at least one wavelength if they are to be resolved (Conyers 2004).

Figure 3 represents the resolved limit (separated by one wavelength), the Rayleigh limit (separated by half the wavelength) and the unresolved events.

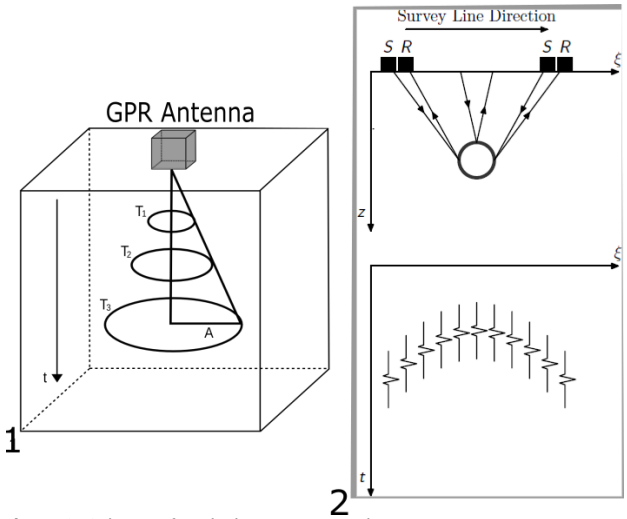

Figure 2: Scheme of conical wave propagation.

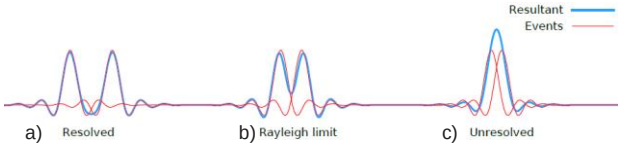

Figure 3: Schematic representation of resolution limits. a) Resolved limit; b) Rayleigh limit; c) Unresolved limit.

The Rayleigh limit consists on the minimal separation for which two point sources can be distinguished.

When there is a resolved signal amplitude is possible to estimate efficiently the reflection of the top and bottom of root target through the GPR signal processing.

The signal amplitude can be interpreted as the result of the surface integer of the target, which depends on the dimensions in three directions.

The signal amplitude generated by the root target is equal to the summation of both top and bottom reflections and its resolution limits varies with the diameter and dielectric constant of the root target.

The maximum resolution consists in the best approximation of the real diameter of target based on a specific environment conditions (ε_{soil}) and root water content (ε_{root}).

When the GPR signal passes through a target smaller than the resolution limit it occurs the scattering/diffraction phenomena. **Figure 3-c)**,represents the unresolved limit, which the resultant underestimates the signal amplitude value for diffraction examples.

Results

The results of the transverse electric and the transverse magnetic field of the numerical model is shown below in **Figure 4** for different root diameter (te), in **Figure 5** for different root diameter (tm), in **Figure 6** for different root dielectric constant based in water content (te) and in **Figure 7** for different root dielectric constant based in water content (tm).

In these cases below, the dielectric constant of the soil was ε_{soil}= 3. The central frequency of the antenna used was 2600 MHz. The average depth of the sample was 15cm. For the diameter variation results was fixed a ε_{root}= 4.5 while for the dielectric constant variation results (ε_{root}) was fixed a diameter of 5cm.

The maximum resolution of vertical features is roughly equivalent to or larger than half the wavelength (Neubauer et al. 2002).

Using the equation (4) to get (5):

$$V = \frac{c}{\sqrt{\varepsilon}} \text{ (4)}$$

$$\lambda = \frac{c}{f.\sqrt{\varepsilon_s}} \text{ (5)}$$

$$\lambda = \frac{0.3}{2.6\sqrt{3}} = 0.066617 \text{ m}$$

According to Neubauer *et al.* (2002):

$$\frac{\lambda}{2} = 3.33\text{cm}$$

The maximum resolution of vertical features in the numerical models was for samples equivalent or larger than 3.33cm in diameter.

The maximum resolution of horizontal features is roughly equivalent to equation(5): 1.665425

$\therefore$

$$A = \frac{6.6617}{4} + \frac{15}{\sqrt{3+1}} = 9.16 \text{ cm}$$

The maximum resolvable horizontal target is equivalent to A, the long dimension of the footprint (Conyers 2004).

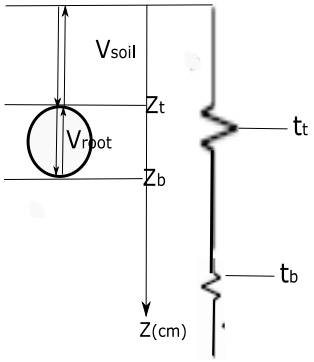

Figure 4: Schematic representation electromagnetic wave interaction.

Figure 4 shows the interaction of the electromagnetic wave. The value of Tt = time of wave reflection arrival of top root sample and the value of Tb= time of wave reflection arrival of bottom root sample were possible to estimate through the following relations:

$$Tt = \frac{2.Zt}{Vsoil} \text{ (6);}$$

Using equation (4) into (6):

$$Tt = \frac{2.Zt.\sqrt{\varepsilon}soil}{c} \text{ (7);}$$

Similarly,

$$Tb = Tt + \frac{2.(Zb-Zt).\sqrt{\varepsilon}root}{c} \text{ (8);}$$

Where Zb-Zt = d (sample diameter).

Resolving for the maximum resolution limit (Neubauer *et al.,* 2002):

$$\frac{2.d.\sqrt{\varepsilon}root}{c} < \frac{c}{2.f.\sqrt{\varepsilon}soil},$$

$$d < \frac{c^2}{4.f.\sqrt{\varepsilon}soil.\sqrt{\varepsilon}root}, \text{ (9)}$$

From equation (9) the diameter of root sample has to be lower than this relationship to be resolved for the maximum resolution limit.

Similary it is possible to get:

$$\sqrt{\varepsilon}root < \frac{c^2}{4.f.\sqrt{\varepsilon}soil.d} \text{ , (10)}$$

From equation (10) the dielectric constant of root sample has to be lower than this relationship to be resolved for the maximum resolution limit.

The signals amplitude showed in **Figure 5**-1a), 1b) and **Figure 6**-1a), 1b) are diffractions examples due to the size diameter of the root target and the environment characteristics.

The signals amplitude showed in **Figure 5**-2a), 2b), 3a), 3b),4a), 4b) and **Figure 6**-2a), 2b), 3a), 3b), 4a), 4b) are reflections examples due to the size diameter of the root target and the environment characteristics.

Higher water content in roots than in soil matrix can provide the necessary permittivity contrast, making root detection by GPR possible (Cui *et al.,* 2011). Dried roots are difficult to be detect by GPR. If the volumetric content of water by weight is less than 20%, detection becomes impossible, while roots with approximately 50% content are clearly identified (Hirano *et al.*, 2009).

According to the **Figures 7** and **8**, the signal amplitude increases with the increasing of the dielectric constant of the root (ε_{root}). The **Figure 7**-1a), 1b) and **Figure 8**-1a), 1b) have a phase inversion in comparison to the other examples. The reason is the lower ε_{root} [2] than the ε_{soil} [3].

Conclusions

This paper shows Reflexw feasibility in exploring the impacts of limiting factors on root diameter and root water content variation for the transverse electric field and the transverse magnetic field.

The numerical modeling experiment showed consistent results. It is possible to estimate the variables (target diameter, target depth, target dielectric constant and the environment dielectric constant) to understand the electromagnetic wave propagation and interaction in subsurface.

Through the experiment was possible to estimate the expected size of the event and the minimum size of a sample to be imaged by a GPR system. The experiment also showed that the variation of the dielectric constant of the root plays a key role on the estimation of the root diameter, which is an important index for the best estimation of root biomass.

References

al-Hagrey, S.A. (2007) Geophysical imaging of root-zone, trunk, and moisture heterogeneity. J Exp Bot 58:839–854 doi:10.1093/jxb/erl237

Annan, A.P., 1992. Ground penetrating radar workshop notes. Sensors; Software, Inc., Internal Report, 130p.

Annan, A.P. 2009 Electromagnetic Principles of Ground Penetrating Radar. In Ground Penetrating Radar: Theory and Applications, edited by Harry M. JoI, pp. 3-40. Elsevier, Amsterdam.

Barton, C.V.M. & Montagu, K.D. (2004) Detection of tree roots and determination of root diameters by ground penetrating radar under optimal conditions. Tree Physiol 24:1323–1331. doi:10.1093/treephs/24.12.1323.

Conyers, L. B. & Goodman, D. 1997. Ground-Penetrating Radar: An Introduction for Archaeologists. Walnut, Creek, CA: AltaMira Press.

Conyers, L.B. 2004. Ground-Penetrating Radar for Archaeology. Altamira Press, Walnut Creek.

Cui, X.; Chen, J.; SHEN, J.; CAO, X.; CHEN, X.; ZHU, X. Modeling tree root diameter and biomass by ground-penetrating radar. Science China Earth Sciences. May 2011. Vol. 54 No.5: 711-719 doi:10.1007/s11430-010-4103-z.

Dannoura M, Hirano Y, Igarashi T, Ishii M, Aono K, Yamase K, Kanazawa Y (2008) Detection of Cryptomeria japonica roots with ground penetrating radar. Plant Biosyst 142:375–380. doi:10.1080/11263500802150951.

Du S & Rummel P., 1994. Reconnaissance Studies of Moisture in the Subsurface with GPR, In: Proceedings of The Fifth International Conference on Ground Penetrating Radar, GPR 94, p. 1241–1248.

Guo, L.; Lin, H.; Fan, B.; Cui, X.; Chen, J. Forward simulation of root's ground penetrating radar signal: simulatior development and validation. 2013. Plant Soil. DOI 10.1007/s11104-013-1751-8.

Hirano, Y., Dannoura, M., Aono, K. et al. Limiting factors in the detection of tree roots using ground-penetrating radar. Plant Soil (2009) 319: 15.

Hruška J, Cermák J, Sustek S (1999) Mapping tree root systems with ground-penetrating radar. Tree Physiol 19:125–130. doi:10.1093/treephs/19.2.125

Neubauer, W., A. Eder-Hinterleitner, S. Seren, and P. Melichar. 2002. Georadar in the Roman Civil Town Carnuntum, Austria: An Approach for Archaeological Interpretation of GPR Data. Archaeological Prospection 9:135-156.

Sandmeier, K.J. 2015 REFLEXW. Version 6.0. WindowsTM 9x/NT/2000/XP/7 – program for the processing of seismic, acoustic or eletromagnetic reflection, refraction and transmission data. Manual. 516p.

Taflove, A. 1995. Computational Electrodynamics: The Finite-Difference Time-Domain Method. Artech House.

Torgovnikov, G.I. 1992. Dielectric properties of wood and wood based materials. Springer, Berlin, Heidelberg, New York.

Wensik, W.A. 1993. Dielectric properties of wet soils in the frequency range 1 - 3000 MHz. Geophysical Prospecting, 41: 671-696.

Yilmaz, O. 1987. Seismic Data Processing. SEG. Sheriff,R.E. & Geldart, L.P., 1982. Exploration Seismology. Volumes 1 & 2. Cambridge University Press.

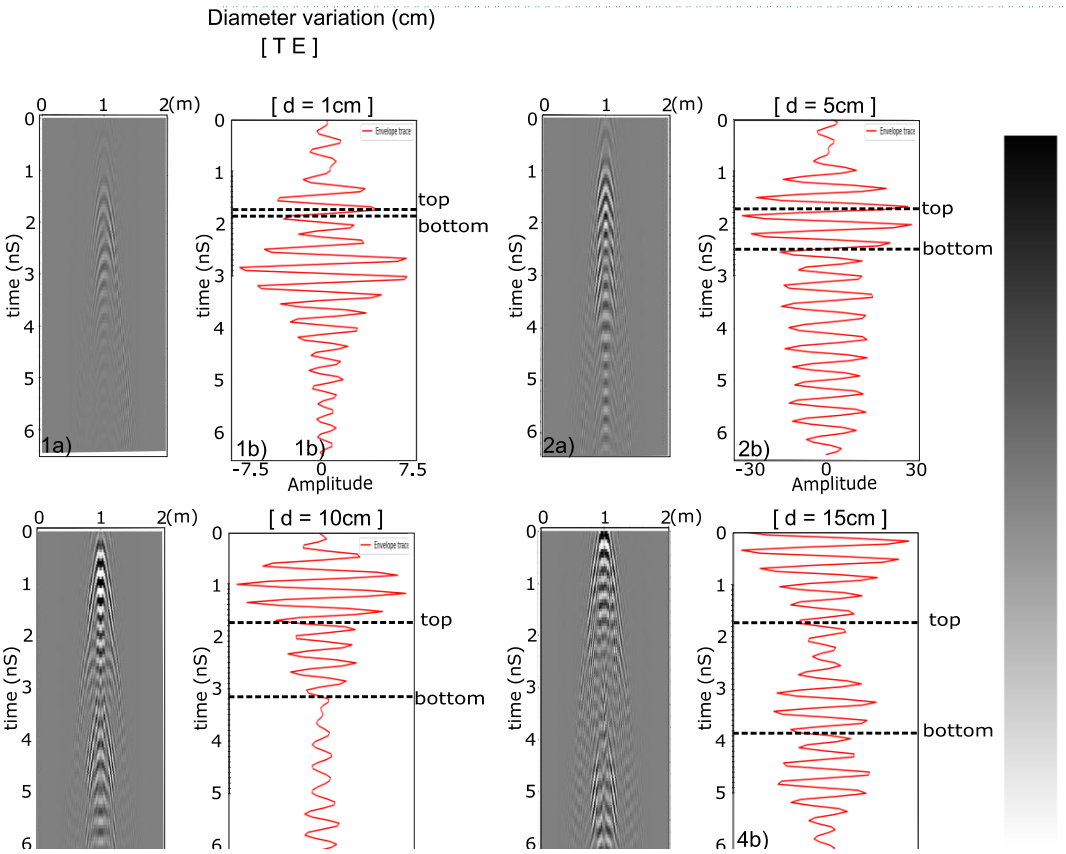

Figure 5 : Target diameter variation for the transverse electric field.

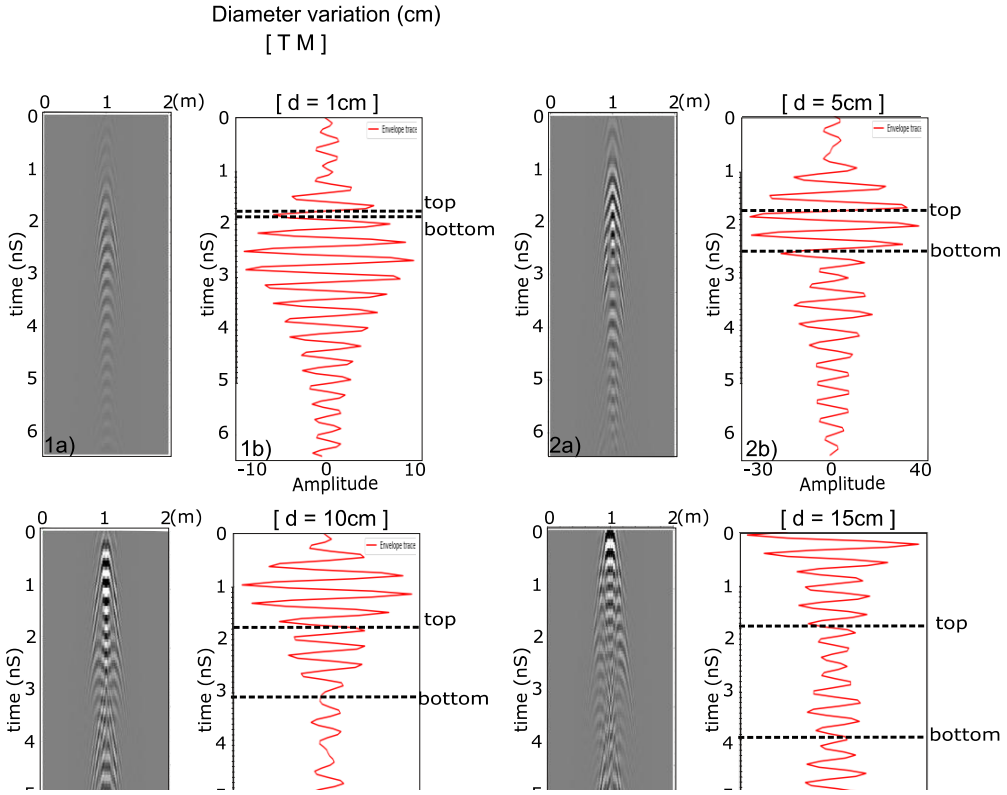

Figure 6: Target diameter variation for the transverse magnetic field.

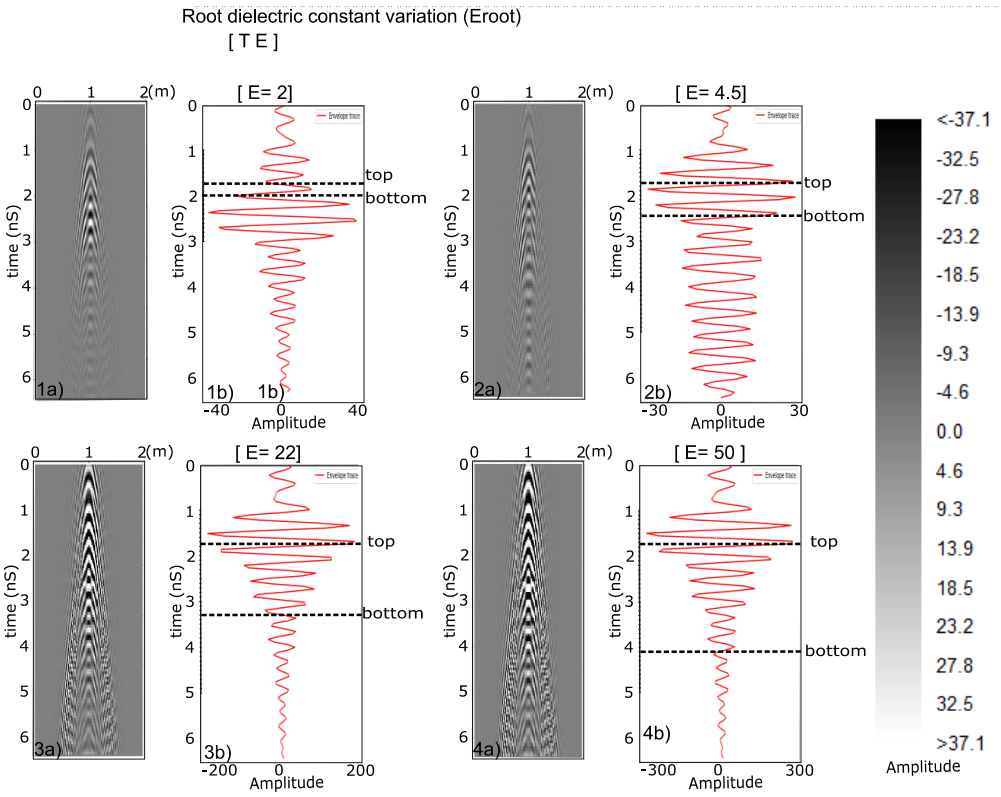

Figure 7: Target dielectric constant variation for the transverse electric field.

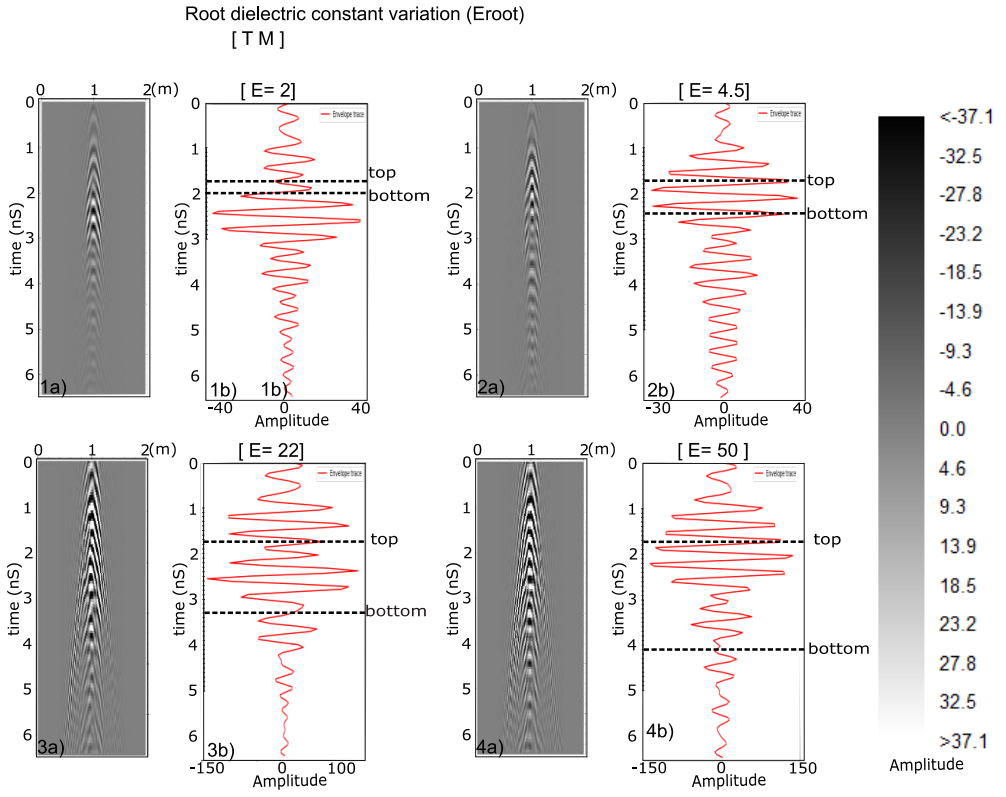

Figure 8: Target dielectric constant variation for the transverse magnetic field